



Mesoscale functional connectivity in macaque visual areas[☆]

Xingya Cai¹, Haoran Xu¹, Chao Han, Peichao Li, Jiayu Wang, Rui Zhang, Rendong Tang, Chen Fang, Kun Yan, Qianling Song, Chen Liang, Haidong D. Lu*



State Key Laboratory of Cognitive Neuroscience and Learning, IDG/McGovern Institute for Brain Research, Beijing Normal University, No. 19 Xin Jie Kou Wai Street, Beijing 100875, China

ARTICLE INFO

Keywords:
Macaque
Visual cortex
Resting state
ISOI
Hemodynamic signal
Functional connectivity
Functional maps

ABSTRACT

Studies of resting-state functional connectivity (rsFC) have provided rich insights into the structures and functions of the human brain. However, most rsFC studies have focused on large-scale brain connectivity. To explore rsFC at a finer scale, we used intrinsic signal optical imaging to image the ongoing activity of the anesthetized macaque visual cortex. Differential signals from functional domains were used to quantify network-specific fluctuations. In 30–60 min resting-state imaging, a series of coherent activation patterns were observed in all three visual areas we examined (V1, V2, and V4). These patterns matched the known functional maps (ocular dominance, orientation, color) obtained in visual stimulation conditions. These functional connectivity (FC) networks fluctuated independently over time and exhibited similar temporal characteristics. Coherent fluctuations, however, were observed from orientation FC networks in different areas and even across two hemispheres. Thus, FC in the macaque visual cortex was fully mapped both on a fine scale and over a long range. Hemodynamic signals can be used to explore mesoscale rsFC in a submillimeter resolution.

1. Introduction

Resting-state brain activity contains rich functional and structural information from which intrinsic functional connectivity (FC) can be decoded (Fox and Raichle, 2007). However, most resting-state fMRI studies have focused on large-scale FC. It is unclear whether mesoscale FC (e.g., horizontal connections among orientation columns in V1) can also be mapped with the ongoing hemodynamic signals. Spontaneous activity within these highly specific FC networks is largely unknown. Recent efforts have been made in the mapping of high-spatial-resolution FC with fMRI, such as determining the borders between brain areas (Wig et al., 2014), topographic projections among brain areas (Jbabdi et al., 2013), and delineation of subareas (Hutchison et al., 2015). Using monkeys, resting state FC has been compared with effective connectivity (Matsui et al., 2011) and anatomical connectivity (Wang et al., 2013); used to explore scene-processing networks (Li et al., 2022) and high-level cognitive networks (Mars et al., 2013; Schwiedrzik et al., 2015). These findings have demonstrated that hemodynamic signals may contain finer-scale information that can be used to study mesoscale FC.

Intrinsic signal optical imaging (ISOI) is based on cortical hemodynamic information and has been used successfully in mapping submillimeter functional architectures in brain areas (Grinvald et al., 1999).

ISOI has also been used in exploring the ongoing brain activity in different species. With ISOI, FC has been obtained from mice (e.g., White et al., 2011), ferrets (Vasireddi et al., 2016), and New World monkeys (Card et al., 2022). To our knowledge, however, the ISOI has not been used on Old World monkeys for mapping FC. Nonhuman primates are important animal models for resting-state studies (Hutchison and Everling, 2012). Particularly, macaque visual areas have been used as a model system for human vision. Previous anatomical work has shown rich mesoscale connections in macaque visual areas, such as grid-like horizontal connections among orientation columns (e.g., Malach et al., 1993). A recent VSD study also revealed that mesoscale connectivity rules can be detected in macaque V1 (Omer et al., 2019, also see Tsodyks et al., 1999). It is unknown whether these highly specific functional networks can be observed in ongoing hemodynamic signals, as well as their potential impacts on the large-scale FC observed with fMRI (e.g., Vincent et al., 2007).

To answer these questions, we used ISOI to image the ongoing activity of visual areas V1, V2, and V4 in anesthetized macaques. We quantified spontaneous activity patterns in these areas and compared them with the activation maps collected with visual stimulation. We further analyzed the temporal relationships of these patterned fluctuations within and across these three areas.

[☆] <https://lulab.bnu.edu.cn/enhome/>

* Corresponding author.

E-mail address: haidong@bnu.edu.cn (H.D. Lu).

¹ These authors contributed equally to this work.

2. Materials and methods

2.1. Animals

Data were collected in collaboration with other research projects. We performed short spontaneous imaging before the main imaging sessions for different projects and animals. For this study, thirteen cases that met the following criteria were used: 1. Clear visual response maps gathered in visual stimulation sessions; 2. More than two visual areas exposed in the imaging field of view. These thirteen cases (seven left hemisphere cases, five right hemisphere cases, and one bi-hemisphere case) were from twelve adult male macaque monkeys (nine *Macaca mulatta* and three *Macaca fascicularis*, 5–7 years old, weighing 4.6–9 kg). All thirteen cases contained area V1, among which eleven cases had V2, and six cases had V4. All surgical and experimental procedures conformed to the guidelines of the National Institute of Health and were approved by the Institutional Animal Care and Use Committees of Beijing Normal University and Institute of Neuroscience, Chinese Academy of Sciences.

2.2. Surgery & anesthesia

Chamber implant and imaging preparation procedures were the same as previously described (Li et al., 2013). In the imaging experiments, monkeys were initially tranquilized with ketamine (10 mg/kg, i.m.) in the cage together with atropine sulfate (0.05 mg/kg, i.m.). They were then transferred to the lab. After intubation, they were placed in a stereotaxic apparatus and artificially ventilated with 1–2.5% isoflurane during the preparation. Before imaging, monkeys were paralyzed with vecuronium bromide (induction 0.25 mg/kg; maintenance 0.05 mg/kg/h, i.v.) and anesthesia was switched to propofol (induction 5 mg/kg, maintenance 5 mg/kg/h i.v.) (for five cases), or a mixture of propofol (induction 2 mg/kg, maintenance 2 mg/kg/h i.v.) and sufentanil (induction 0.15 µg/kg, maintenance 0.15 µg/kg/h i.v.) (for six cases), Zoletil (induction 1.5 mg/kg, maintenance 1.5 mg/kg/h, for one case), or Ketamine (induction 10 mg/kg, maintenance 10 mg/kg/h, for one case). Anesthetic depth was assessed continuously by monitoring heart rate (140–200 beats per minute), blood oximetry (98–100%), end-tidal CO₂ (4.5–5.5%) and body temperature (38 °C).

2.3. Intrinsic signal optical imaging (ISOI)

In all cases, the spontaneous imaging sessions were performed before any visual stimulus sessions. In twelve cases, the monkey's eyes were closed. In one case, the monkey's eyes were open but covered with a black cloth.

The cortex was illuminated with 632 nm red light, and reflectance images were acquired (Imager 3001, Optical Imaging Inc., Germantown, NY) continuously at a 4 Hz frame rate. In four cases, data were collected for 130–180 sec per block for 10–15 blocks, and there was a 10–20-sec interval after each block to save data. In the other nine cases, data were collected continuously for 30–60 min without interruption. Frame sizes were either 504 × 504 pixels or 540 × 654 pixels representing either 19 × 19 mm or 20 × 24 mm of imaged region.

After spontaneous imaging runs, the monkey's eyes were opened or uncovered. Stimulus-driven images were collected as previously described (Li et al., 2013). In each trial, visual stimulus was shown for 3.5 s. Images were collected 0.5 s before stimulus onset and lasted for 4 s. There was an 8-sec interstimulus interval. Stimulus conditions were repeated 20–50 times and were randomly interleaved. The data were used to generate functional maps that were used to construct map templates for image quantification.

2.4. Visual stimulus

The visual stimuli used in this study were the same as those previously described (Li et al., 2013). Visual stimuli were created using

ViSaGe (Cambridge Research Systems) and displayed on a calibrated 21-inch CRT monitor (SONY CPD-G520) running at a 100 Hz refresh rate. The stimuli were full-screen (40 × 30°) and positioned 57 cm from the eyes. For ocular dominance (OD) and orientation maps, drifting square-wave gratings were used. The spatial frequency (SF) of the gratings was 1 or 1.5 cycles/degree, and the temporal frequency was 4 or 5.33 cycles/s. The orientations of gratings were labeled 0° (horizontal), 45° (anticlockwise 45° from 0°), 90° and 135°, and the drifting directions were orthogonal to the grating orientations. A pair of mechanical shutters was placed in front of the two eyes to achieve monocular stimulation. An orientation map was obtained by comparing responses to orthogonal gratings, and an OD map was obtained by comparing responses to monocular stimuli. For color functional map, responses to red–green isoluminant sinewave gratings and black–white sinewave gratings were compared. Gratings were presented in one of two orientations (45° or 135°) and in random directions orthogonal to the grating orientations. The spatial frequency (SF) of the gratings was 0.15 or 1 cycles/degree, and the temporal frequency was 1 or 4 cycles/s. All stimuli were presented in a random sequence.

2.5. Data analysis for stimulus-driven data

2.5.1. dR/R images

Original images were first transformed to dR/R frames: $dR/R = (R - R_0)/R_0$, where R represents the original image, and R_0 represents the average of the first two frames imaged immediately before stimulus onset (prestimulus baseline).

2.5.2. SVM maps

We used a pattern classifier (support vector machine, SVM) for calculating contrast maps between dR/R frames of two stimulus conditions (Xiao et al., 2008; Chen et al., 2016). The MATLAB SVM program was provided by Chih-Jen Lin (LIBLINEAR: A Library for Large Linear Classification, 2008; available at <https://www.csie.ntu.edu.tw/~cjlin/liblinear/>). For each stimulus, only dR/R frames 8–16 were used. The SVM read two groups of dR/R images and calculated the surface that best separated these two groups of data in high-dimensional response space. In the resulting weight map (SVM map), pixel values represent their contribution to the classification. SVM maps were clipped at 2 SD for display.

In this study, we mainly obtained four functional maps: ocular dominance (OD) maps, orientation maps (including 0° vs. 90° and 45° vs. 135°), and color maps (red/green vs. luminance).

2.5.3. Functional map templates

Based on surface blood vessels and ocular dominance patterns, the V1, V2 and V4 regions were identified. Noncortical pixels and pixels overlaying large blood vessels were marked and excluded from the following analysis. SVM maps were then filtered (circular mean filter, high-pass: 50 pixels, low-pass: 8 pixels), and the pixel values were normalized to -1~1 and sorted in ascending order. Based on their sorted and normalized values, pixels were separated into three groups (for OD and orientation templates: black: -1~−1/3; gray: -1/3~1/3; white: 1/3~1; for color templates: black: -1~−1/3; gray: -1/3~1/5; white: 1/5~1. Since color map had fewer white pixels, here we used a wider range for "white" domains comparing to OD and orientation maps.). Binary maps with only black pixels and white pixels were further filtered (low-pass, 8 pixels, to remove isolated pixels) and transformed into binary maps (threshold 0.5). Maps obtained from black and white pixels were used as functional map templates for corresponding domain types (e.g., left and right-eye templates in Fig. 1C).

2.5.4. Shuffled template

Artificial map templates were created based on real maps for control purposes. For a functional map, we first obtained its spatial frequency map and phase map by 2D fast Fourier transform. The pixel values in the

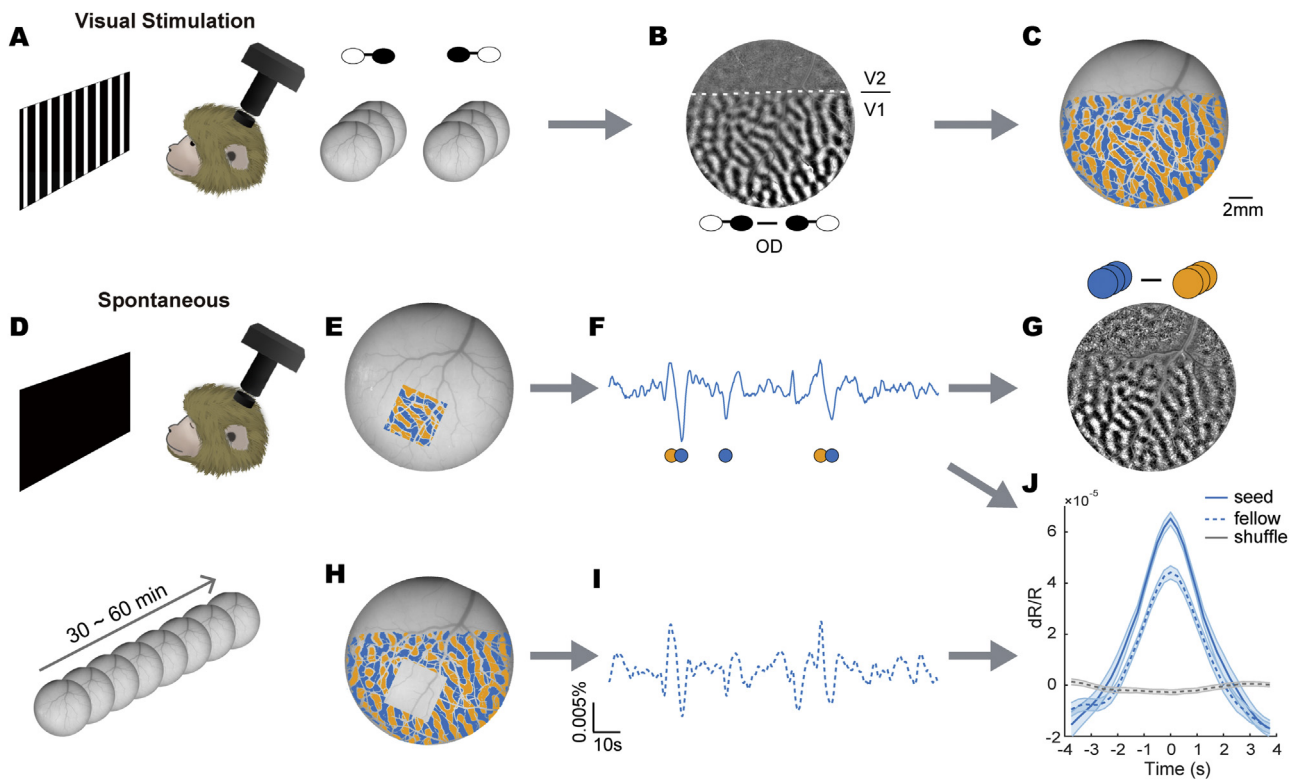


Fig. 1. Imaging and analysis procedures under visual stimulation and spontaneous conditions. A. Illustration shows ISOI of cortical response to visual stimuli and examples of frame sequences recorded under monocular stimulation. B. Ocular dominance (OD) map obtained by comparing cortical responses (right panel in A) to two monocular stimuli. C. OD template in which blue and orange regions contain pixels preferentially driven by left- or right-eye stimuli. D. ISOI of cortical spontaneous activity (usually lasted 30–60 min). The array of gray frames illustrates continuous spontaneous imaging. E. A seed region covered with OD template from (C). F. A 2-minute section of the OD differential signal time course obtained from the seed region shown in (E). Peaks/troughs meet the criterion (see Method) were identified and labelled with orange and blue circles separately. G. A recovered OD map obtained by comparing peak frames and trough frames. It had an OD pattern similar to that obtained with monocular stimuli (B). H. The non-seed region in V1 covered with OD template from (C), which is complementary to (E). I. OD differential signal time course from the non-seed region aligned with the one from the seed region. J. Aligned peaks ($n = 60$) for seed (solid line), fellow (dotted line), and shuffle (gray line) time courses. Curve shading: SEM (same below). Note that the fellow curve also has a peak, although fellow peaks were obtained using the peak times of the seed time course.

phase map were randomized, and the frequency map was rotated for a random angle. These two modified maps were then transformed back to a map using 2D inverse fast Fourier transform (e.g., Fig. S1C). We then performed the same template procedure on this artificial map to obtain an artificial map template (shuffled template). For each control test, 1000 shuffled templates were created. Signals obtained with shuffled templates represents artificial signals induced by the spatial subtraction method. Thus, a real signal (obtained with a real template) needed to be significantly larger than the shuffled signals in order to be considered valid.

2.6. Data analysis for spontaneous data

2.6.1. dR/R images

Raw frames were first transformed to dR/R frames using the following formula: $dR/R = (R - R_0)/R_0$, where R represents the raw frame and R_0 represents the average frame of the whole spontaneous imaging sequence.

2.6.2. Pixel detrending

To remove the slow drift of the signal, we high-pass filtered the time course of each pixel (6th order Butterworth filter, low-cut-off: 0.05 Hz).

2.6.3. Spatial filtering

Detrended frames were filtered (circular mean filter, high-pass: 50 pixels; low-pass: 2 pixels). Each pixel represented 25 to 32 μm of the

cortex. For the bi-hemisphere case, the resolution was 37 $\mu\text{m}/\text{pixel}$. Fifty pixels approximately equal to 1.25 mm.

2.6.4. Differential signal time courses

Differential signal time courses were obtained by subtracting the average pixel values of paired map templates frame by frame. This procedure also removed the global signal which usually had a much larger fluctuation amplitude. For example, in Fig. 1F, the OD differential signal time course was the time-dependent change in the differential between the averaged left-eye pixel value and the right-eye pixel value (Fig. 1E). Similarly, orientation and color differential signals can be calculated from the same data. For each time course, we performed a Fast Fourier Transform (FFT) on the data and, if a breathing noise was significant, removed the breathing noise (typically peaked at 0.5 Hz) using a notch filter (6th Butterworth filter). The time courses were then smoothed with a moving average filter (5 frames, 1.25 s).

2.6.5. Peak-aligned curves

To analyze the spontaneous events, peak-aligned curves were obtained from differential signal time courses. We used two methods to select peaks from the curve. In the first method, we identified the highest N peaks from N-minute imaging (i.e., average of 1 peak per minute). We tested a range of peak numbers, from 0.25 to 4, all worked well (significant recovered map, significant peak height). The choice of 1 peak/min was a tradeoff between signal strength and variance. For strong signal cases, we found a single peak was enough to obtain significant results.

The second (threshold) method was only used for Fig. S2D, in which we estimated the average frequency of peaks (here mean stronger spontaneous fluctuation events) across the imaging. In this method, we calculated a threshold for peak detection. First, we obtained 1000 shuffled differential time courses by creating 1000 shuffled templates as described above. Next, absolute differential signal values of each time course that corresponds to the top 0.5 percentile were determined. Then, the average of 1000 such values from the 1000 shuffled time courses was considered as the strength of background noise and used as the threshold for peak and trough detection from differential signal time courses. Finally, the frequency of peaks was calculated as the total number of peaks and troughs divided by the length of imaging.

For each spontaneous event detected, we selected 15 values on each side of the peak (total 31 values, 7.75 s). Troughs were also detected in a similar way and reversed to be combined with the peaks. The peaks and reversed troughs were aligned and averaged to form a "seed peak" (e.g. solid line in Fig. 1J).

A peak-aligned curve can also be calculated using peak/trough time points belonging to another time course. In Fig. 1J, for example, the fellow peak (dotted line) was obtained from the differential signal time course of the non-seed V1 region (Fig. 1H) but based on peak/trough time points of the seed peaks. This method was used to evaluate the strength of correlated activity in these two differential signal time courses. In these circumstances, we call the time course providing peak/trough times "seed time course", and the one used the peak/trough times to construct peak-aligned curves "fellow time course". The seed and non-seed region could be either parts of a cortical area (e.g., Fig. 2) or different cortical areas (e.g., Fig. 3) for different purposes. For better comparisons, the amplitude of the seed peak was normalized to 1, and the fellow peak was normalized to its own seed peak (e.g., Fig. 2C).

Besides peak-based methods, we also tried analysis based on the whole differential signal time courses. For example, by directly calculating Pearson correlations between seed and fellow time courses. Our analysis indicated that such a correlation method and the peak-based method yielded comparable results. In this paper, we used peak-based method for its better performance for weak signals and for calculating recovered maps (described below).

2.6.6. Recovered maps (Peak-minus-trough maps)

We obtained a recovered map by comparing peak frames and trough frames using an SVM algorithm (e.g., Fig. 1G). The SVM procedure was the same as described above. For frame selection, we used a variable frame range that equaled the width at half-height of a peak/trough. In cases where the numbers of peak and trough frames were not the same, randomly selected frames in the fewer group were duplicated to make them equal.

2.6.7. Correlation coefficients between maps

We used two-dimensional correlation to evaluate the similarity between recovered maps and corresponding functional maps based on the following formula:

$$r = \frac{\sum_m \sum_n (A_{mn} - \bar{A})(B_{mn} - \bar{B})}{\sqrt{(\sum_m \sum_n (A_{mn} - \bar{A})^2)(\sum_m \sum_n (B_{mn} - \bar{B})^2)}}$$

in which array A_{mn} (m and n represent the dimensions of image) and B_{mn} are the images for comparison. \bar{A} and \bar{B} are the means of A and B. Before calculation, noncortical pixels and pixels overlaying large blood vessels or irrelevant cortical area were marked and excluded.

2.6.8. PCA & ICA analysis

We used principal component analysis (PCA) and independent component analysis (ICA) to verify the main results obtained in pixel averaging analysis. Due to the large data size, we first performed PCA to reduce the data dimensions. PC numbers were determined based on experience and trial-and-error. Normally, we kept the first 90–600 principal

components, which accounted for 70–97% of the total data variance. The selected PCs were whitened (each component was divided by its standard error). These data were then used for ICA analysis (FAST ICA: <http://research.ics.aalto.fi/ica/fastica/>) (Hyvärinen and Oja, 2000). We obtained the same numbers of ICs as input PCs. Each IC contains one map and one time course. Visually, there were three types of ICs: the majority of ICs had clear blood vessel signals; some ICs contained function-map-like patterns; and some ICs contained random noises (Fig. 5A).

2.6.9. Response profile

Population response profile (Basole et al., 2003; Chen et al., 2016) was calculated to assess the overall orientation response in a particular IC functional map (Fig. 5C). Briefly, the orientation angle map obtained from a vector analysis (Bosking et al., 1997) was used as the reference angle map. For a specific IC functional map under examination, the top 40% of pixels in a magnitude map from a vector analysis were categorized into 20 orientation-selective groups (0–180°) according to their orientation angles in the reference angle map. Pixel values within each group were then summed and fitted with cosine function. The resulting response profile reflects whether a map contains specific orientation information.

3. Results

We examined spontaneous activities from visual areas in twelve macaques, which were shared with other research projects. The optical window (14–18 mm in diameter) covered parts of V1, V2, and/or V4. During each experiment, imaging of spontaneous activity was always performed before other imaging sessions. The animal's eyes were closed or covered, and the lights were turned off. Continuous imaging usually lasted 30 to 60 min at a frame rate of 4 Hz (total of 7000 to 14,000 frames). After the spontaneous imaging session, stimulus-driven sessions were performed, during which cortical responsiveness was evaluated and functional maps, including ocular dominance (OD) maps, orientation maps, and color maps, were generated. Based on these maps, domain templates were obtained for subsequent quantification (Fig. 1A–C).

3.1. Coherent spontaneous patterns in V1

The raw data acquired in the spontaneous session were first preprocessed, including dR/R, detrend, and spatial filtering (detailed in Methods). Subsequently, "differential signal time course" and "recovered maps" were examined, as illustrated in Fig. 1D–J. In this study, we focused our analysis on these differential signals between domain types. The global signal contained large noise that would obscure the fine-scale spatial information and was removed in the calculation of the differential signals.

We first examined area V1. The differential signal time course (Fig. 1F) was calculated from a V1 seed region using the OD template (Fig. 1E): In each spontaneous frame, right-eye pixels in the seed region were averaged and subtracted from the average of the left-eye pixels. This 60-min long OD curve fluctuates over time. We then identified the 60 highest peaks and troughs from this curve. For each peak, "peak frames" (within half-height range) were selected, and all these "peak frames" were pooled and compared with the "trough frames" using an SVM classifier. The resulting "recovered OD map" (Fig. 1G) exhibited a regular OD pattern that resembled the OD pattern obtained with monocular stimulation (Fig. 1B). Two maps (Fig. 1B & G) had a good correlation ($r = 0.62$). The same procedures but using an artificial template resulted in a flat map (Fig. S1C and D), which indicates that the regular OD pattern was not a random effect. Importantly, the OD pattern also appeared outside the "seed region" but did not cross the V1–V2 border. All the evidence indicates that OD FC exists in ISOI spontaneous images.

We averaged all the peaks and reversed troughs from the seed OD time course and obtained an aligned "seed peak" (solid blue curve in

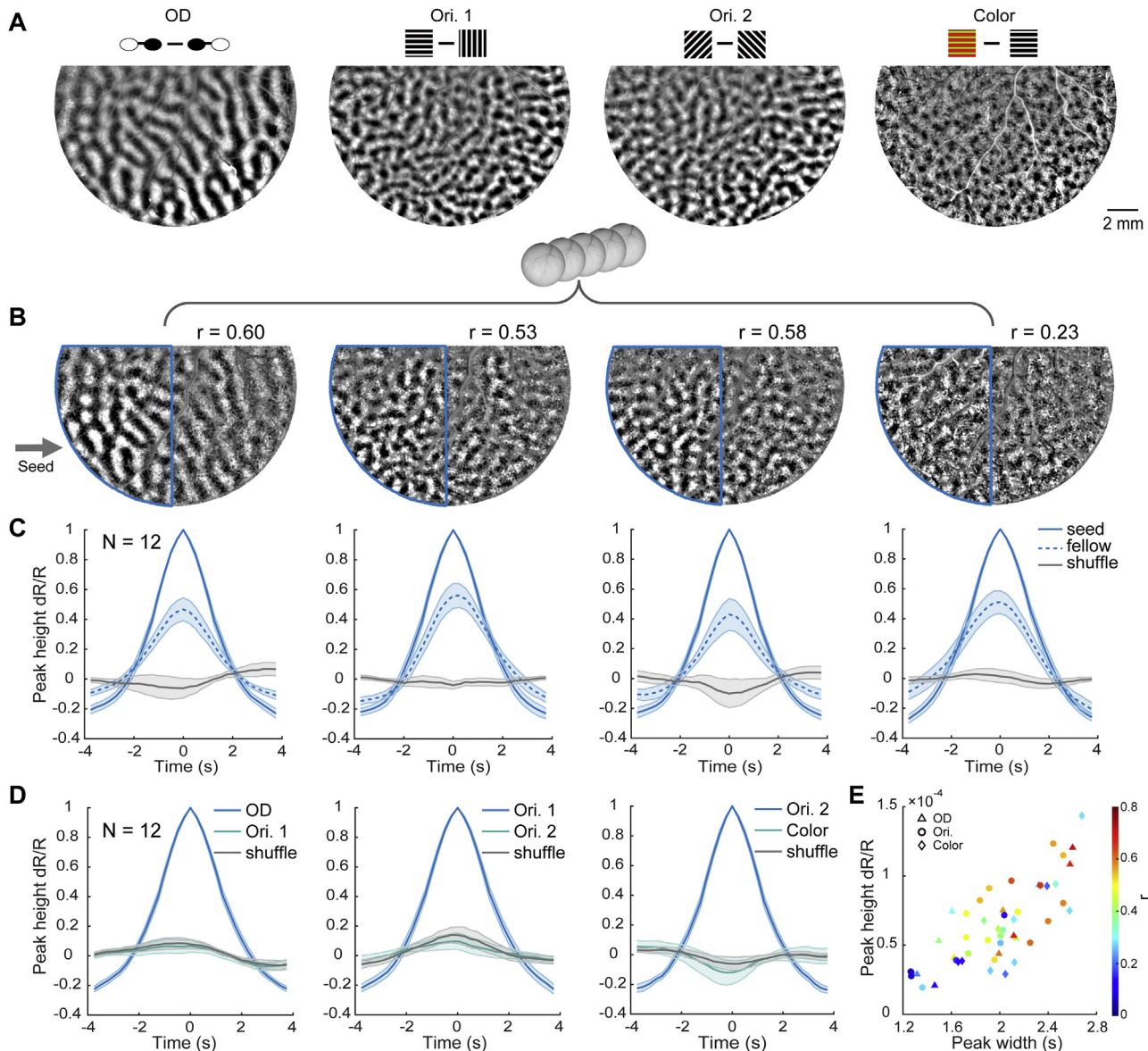


Fig. 2. Spontaneous maps from V1. A. Ocular dominance (OD), orientation (Ori.) and color maps obtained with visual stimuli. B. Spontaneous maps obtained with the same procedures described in Fig. 1G. The seed regions were left half of V1 (blue outlines). Similarity of the non-seed region of these maps with corresponding functional maps (A) was evaluated with two-dimensional correlation analysis (correlation coefficients shown on top of the maps). C. Aligned peaks for seed (left side V1), fellow (right side V1), and shuffle differential signal time courses for four types of map templates, averaged from twelve V1 cases. For each case, a peak curve was normalized by the amplitude value of the seed peak of the corresponding region and template (same below). D. Aligned peaks for nonmatched time courses. Taking the left panel as an example, the blue curve was obtained from OD peaks, while the green curve was obtained from the Ori.1 differential signal time course using the peak times of OD peaks. The gray curve was obtained from the shuffled differential time course using the same peak times from the OD peaks. All nonmatched curves show insignificant differences from shuffle curves ($p > 0.1$, Wilcoxon rank sum test). E. Scatter plot of half-height width and height of averaged peaks from all analyzed V1 cases ($N = 12$). Each case contributed four datapoints based on four map templates. The color of the symbols represents the similarity between the recovered maps and their corresponding functional maps.

Fig. 1J). This averaged peak represents the fluctuation strength of the OD network within the seed region. Based on an OD template for the complementary region (non-seed region), we obtained another OD time course (Fig. 1I). From this time course, sections aligned with those seed peaks/troughs were selected and averaged (dotted line in Fig. 1J). This “coaligned” curve also had a peak that aligned with the seed peak. We call this coaligned peak a “fellow peak”. Consistent with the observation of the OD pattern in the recovered map (Fig. 1G), the presence of a “fellow peak” indicates that the two time courses have coherent activation. As expected, a coaligned curve using a shuffled template did not have a peak (gray curve in Fig. 1J).

3.2. Coexistence of different FC networks in V1

From the same 60-min spontaneous images, we identified a series of FC patterns based on different types of map templates. Fig. 2A shows four functional maps obtained with grating stimuli. With templates from these maps (not shown) and half the V1 as the seed region (blue outlined regions in Fig. 2B), we obtained four recovered maps (Fig. 2B). Among these maps, the OD and orientation recovered maps had FC patterns that were similar to the original maps ($r > 0.5$, for non-seed regions), while the color recovered map in this case had a lower correlation ($r = 0.23$). More examples of recovered OD maps in other cases were

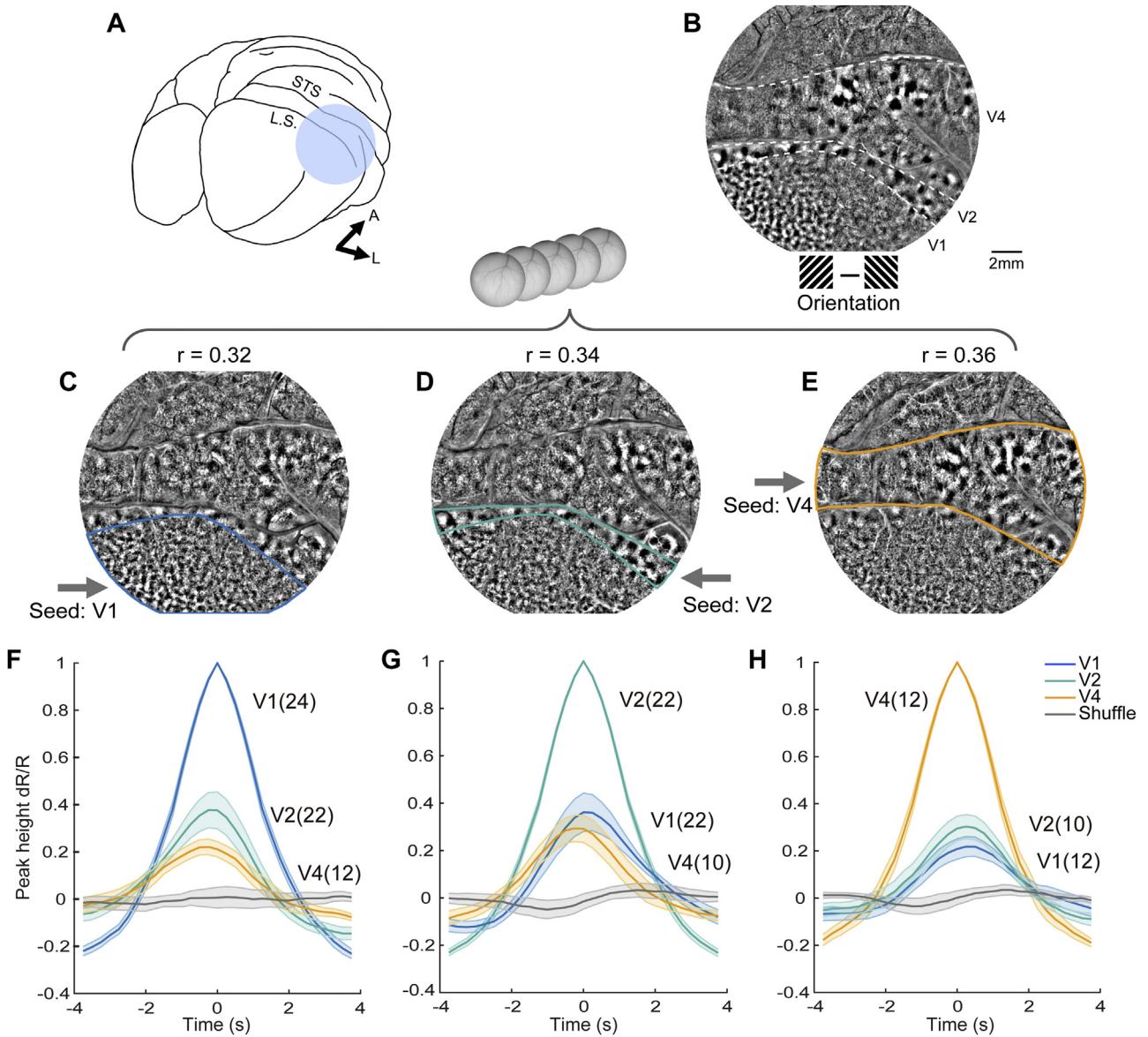


Fig. 3. Spontaneous orientation maps from V1, V2, and V4. **A.** An illustration of a monkey brain with an imaging window (blue disk) that covers parts of V1, V2, and V4. L.S., lunate sulcus; STS, superior temporal sulcus. **B.** A stimulus-driven orientation map (45° vs. 135°) of an example case, which shows orientation domains in all three areas. **C-E.** Orientation maps recovered from the same spontaneous images with 45° vs. 135° seeds in V1, V2 and V4, respectively. Correlation coefficients between recovered maps in non-seed regions with the corresponding functional maps are shown above. **F-H.** Aligned peaks from seed, fellow, and shuffle differential signal time courses for V1, V2 and V4. Due to the variation of exposed areas in the field of view from case to case, these graphs have different numbers of curves used for averaging: For V1 seed: Nv1=24; Nv2=22; Nv4=12; For V2 seed: Nv1=22; Nv2=22; Nv4=10; For V4 seed: Nv1=12; Nv2=10; Nv4=12. N represents the curve numbers used for averaging, including both 45° vs. 135° and 0° vs. 90° curves for each case. For each case, a peak curve was normalized by the amplitude value of the seed peak of the corresponding region and template.

shown in Fig. S1. Fig. 2C shows normalized seed and fellow peaks averaged from all twelve V1 cases. The fellow peaks were approximately half the height of the seed peaks, but all were significantly higher than the shuffled control (Wilcoxon signed rank test, $p < 0.001$; also see Fig. S3A). Peaks from different time courses were similar (Fig. S2): small amplitudes (dR/R : 0.01%), which were approximately 1/10 of the differential signal in stimulus conditions (Lu et al., 2017), symmetrical waveforms, short durations (~ 4 s), and low occurring frequencies (average ~ 0.02 Hz, measured with another peak detection method, see Fig. S2D).

Fig. 2E shows a population distribution of peak heights and widths for all V1 cases. These were measured from peaks using the whole V1 as the seed. Peak heights and widths were positively correlated, and both were correlated with the strength of the recovered map patterns (color of

the symbols). Different cases had a largely scattered distribution. Some cases had insignificant fluctuations, and their recovered maps did not have an apparent pattern (e.g., Fig. S1B case 3, Fig. S6D).

For each case, although OD, orientation and color patterns were derived from the same spontaneous imaging (30~60 min), these different networks fluctuated independently. Fig. 2D shows pooled results of all twelve V1 cases, each case used whole V1 as the seed. As we can see, the fellow peaks from the orientation time course were flat when non-matching peak times were used for alignment (e.g., from the OD time course, first panel of Fig. 2D). These non-matching fellow peaks were not significantly different from shuffled controls (all $p > 0.1$, Wilcoxon sign rank test, also see Fig. S3B). In addition, the 0° vs. 90° orientation network and the 45° vs. 135° orientation network did not temporally correlate in their fluctuations (Fig. 2D).

3.3. Coherent activity between visual areas

In all visual areas examined (V1, V2, and V4), we observed spontaneous orientation maps. We then investigated temporal relationships between these orientation networks. Fig. 3A-B shows an example case in which all three areas were visible in the field of view. Orientation maps were obtained in all three areas in visual-stimulation runs (Fig. 3B). We used 45° vs. 135° orientation templates in each of the three areas as seeds and obtained three recovered maps (Fig. 3C-E). All three maps show orientation patterns not only in the seed areas but also in the other two areas (V1 as seed, $r = 0.29 \pm 0.20$; V2 as seed, $r = 0.24 \pm 0.17$; V4 as seed, $r = 0.17 \pm 0.12$, for non-seed areas. Mean \pm SD). The fellow peaks were all significantly higher than those of the shuffled controls ($p < 0.01$, Wilcoxon signed rank test, Fig. 3F-H). These results indicate that the matched orientation networks in different areas had correlated spontaneous fluctuations, likely due to a hierarchical transfer of feature-specific information. We also performed the same analysis using color templates. Unlike orientation, recovered color maps were very weak ($r = 0.05 \pm 0.09$, for non-seed areas). This may be due to weak color activation in each individual area (e.g., color map in Fig. 2B and Fig. S6).

3.4. Coherent spontaneous activity across hemispheres

We further examined whether spontaneous activity synchronized across the two hemispheres. In one case, we exposed V1 in both the left- and right-hemispheres and imaged both regions in one field of view (Fig. 4A and B). We used left-V1 as a seed and examined activity in right-V1. With the left OD template, a clear OD pattern and a strong fellow peak were obtained from right-V1 (Fig. 4F and I), indicating the existence of coherent spontaneous activity across the two hemispheres. With the left orientation template, the orientation pattern in right-V1 was weak but visible (Fig. 4D). A significantly large fellow peak indicates that orientation fluctuation also synchronizes across hemispheres (Fig. 4J). Color coherency was slightly different; although some patterns were present in the recovered map (Fig. 4H, likely due to contamination from OD fluctuation, not observed in other cases), the fellow peak was mainly flat and did not differ from the shuffled control (Fig. 4K). This may be due to the small sizes of color domains and weak spontaneous activity in color networks (see Discussion). In both OD and orientation recovered maps, we noticed that patterns were stronger in regions closer to the V1-V2 border (upper half) than in regions farther away (lower half). This difference is quantified in Figure S4G&H and suggests that coherent activity was achieved through transcallosal connections, which have been demonstrated to be orientation-specific (Rochefort et al., 2007; Cusick and Kaas, 1986; Houzel et al., 2002; Innocenti et al., 2022).

3.5. Blind source analysis

In the above template-based analysis method, a template was required to measure the corresponding spontaneous activation. As a comparison, we additionally used independent component analysis (ICA) to explore whether the same FC patterns can be observed without map templates or any prior knowledge. In the example shown in Fig. 5A, we obtained 90 independent components (ICs). Each consists of a map and a time course. These ICs were sorted in the order of their contribution to the source signal. The higher-ranking ICs normally contained large blood vessel patterns, indicating that blood vessel noise contributed significantly to the spontaneous fluctuation. In lower-ranking ICs, we found that some of the IC maps indeed matched the functional maps (third row in Fig. 5A).

Some IC maps had patterns similar to orientation maps (e.g., four examples shown in Fig. 5B). To verify, we calculated their orientation response profiles. In the case shown in Fig. 5, nine IC maps had strong

orientation responses (Fig. 5C) and had good fitting scores ($R^2 > 0.9$). Note that these nine IC maps had a range of peak orientations, suggesting that different orientation networks activated randomly during spontaneous fluctuation.

In different cases we analyzed with ICA method, OD and orientation ICs were the most frequent ones we observed. Color IC maps were also observed, but in a much lower frequency (V1 color IC map: 2 in 12 cases, V2 color IC map: 1 in 11 cases). This is consistent with the observation that recovered color maps were weak in template-based method (Fig. S3C). In one case we also observed a V2 disparity IC map (1 in 11 cases, left column in Fig. S5B). We did not observe IC maps for direction maps (Lu et al., 2010; Li et al., 2013) or curvature maps (Tang et al., 2020).

For the same data set, both ICA and the template-based method obtained consistent results. For repeatedly imaged chambers, results were also repeatable over different imaging days (Fig. S5A). Taken together, this method could be useful for studying areas that are less explored or are proven difficult to be studied with conventional stimulus/task-based methods.

4. Discussion

To our knowledge, this work represents the first ISOI study of spontaneous activity in macaques. We identified submillimeter-resolution FC networks at different spatial scales (intra- and interareas, across hemispheres). Together with earlier fMRI work (e.g., Vincent et al., 2007; Fox and Raichle 2007), these findings indicate that hemodynamic signals contain FC information at both macro- and mesoscale spatial resolutions. Furthermore, through multiarea imaging, an overall picture of mesoscale FC in the macaque visual cortex was illustrated, including the multiplexed FC networks in each area, their independent temporal fluctuations, and temporal correlations in the orientation networks along the visual hierarchy.

Anatomical horizontal connections are likely the underlying neural substrates for the multiplexed intra-areal FC networks we observed (Smith et al., 2018). Previous V1 tracer studies have revealed preferential connections among the same types of OD columns (Malach et al., 1993; Yoshioka et al., 1996), orientation domains (Malach et al., 1993; Stettler et al., 2002), and CO blobs (Livingston and Hubel, 1984; Yoshioka et al., 1996; Yabuta and Callaway, 1998). In areas V2 and V4, such like-to-like connections are also present (Amir et al., 1993; Malach et al., 1994; Hu and Roe, 2022). Thus, local spontaneous fluctuation can selectively activate nearby neurons of similar preferences. The patchy horizontal connections are generally within 5 mm (Amir et al., 1993; Malach et al., 1993), which is shorter than the extent of the FC patterns we observed (10–20 mm). Apparently, spontaneous activity is relayed within such function-specific networks, probably as traveling-wave forms. In an earlier VSD study, an increase in the size of spontaneous maps over time was indeed observed (Omer et al., 2019). In our results, the decrease in map strengths over distance (e.g., Fig. 2B, also see Fig. S4) is consistent with this conjecture.

Another potential source for FC is common inputs. For example, retinal spontaneous activity is monocular in nature and may provide additional synchrony for V1 neurons receiving inputs from the same eye. In recovered FC maps, the OD maps overall appeared stronger but insignificant than the orientation maps (Figs. 2B and S2C: OD $r = 0.46 \pm 0.20$, orientation $r = 0.42 \pm 0.19$, Mean \pm SD. OD vs. orientation, $p = 0.51$, Wilcoxon rank sum test). In bi-hemisphere imaging, OD patterns appeared stronger and extended further from V1/V2 border than the orientation patterns (Fig. 4D). Thus, the coherent OD fluctuations might also have additional eye-specific drives. However, eye-specific input was unlikely the sole driver of the OD FC, since the recovered OD patterns also showed decay over distance, an indication of horizontal connections. It is more likely that the OD FC was a combined effect of coherent inputs and horizontal connections.

In the monkey visual system, orientation selectivity is generally believed to be developed in V1. Thus, the coherent orientation fluctuation

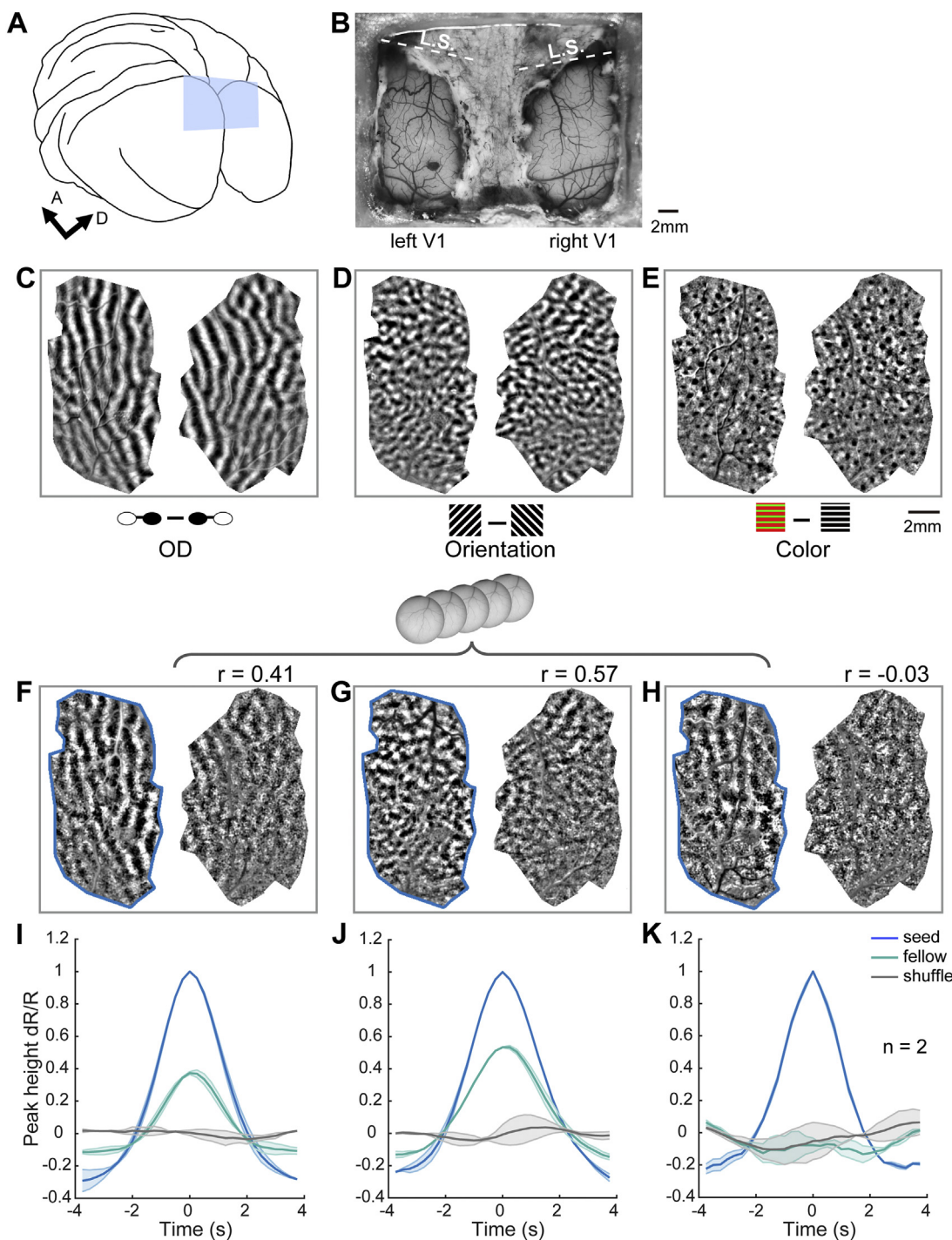


Fig. 4. Spontaneous maps from two hemispheres. **A.** An illustration of a monkey brain with an imaging window (blue rectangle) for two-hemisphere imaging. **B.** Blood vessel map within the imaging window. **C-E.** Functional maps obtained with stimuli: OD map (**C**), orientation map (45° vs. 135°) (**D**), and color map (**E**). **F-H.** Recovered spontaneous maps using different seed maps of the left V1. Correlation coefficients between recovered maps and functional maps (**C-E**) are shown above. **I-K.** Aligned peaks for seed, fellow and shuffle differential signal time courses. For each case, a peak curve was normalized by the amplitude value of the seed peak of the corresponding region and template. Left- and right-V1 differential signal time courses were used as seed time courses in turn before averaging.

along this pathway can only be due to hierarchical transfer, not a “common source”. The ventral visual pathway (V1, V2, and V4) is the major pathway for object shape processing. Our observation also indicates that the parallel pathways built for visual processing can also transfer feature-specific ongoing activity.

It remains unclear how far along the visual stream spontaneous activity can reach. Under normal resting conditions, we do not sense continuous changes in visual sensation. Thus, it is likely that such spontaneous

fluctuation is blocked somewhere in the visual pathway. When a visual stimulus is presented, it has been shown that ongoing feature-specific network activity may interact with the representation and/or transfer of stimulus-related information (Arieli et al., 1996; Scholvinck et al., 2012). Previously, we observed rivalry-like activity in anesthetized monkey V1 (Xu et al., 2016). The multiplexed spontaneous fluctuation could provide a possible drive and continuous influence for this bistable visual perception. Detailed investigation of similarities between these

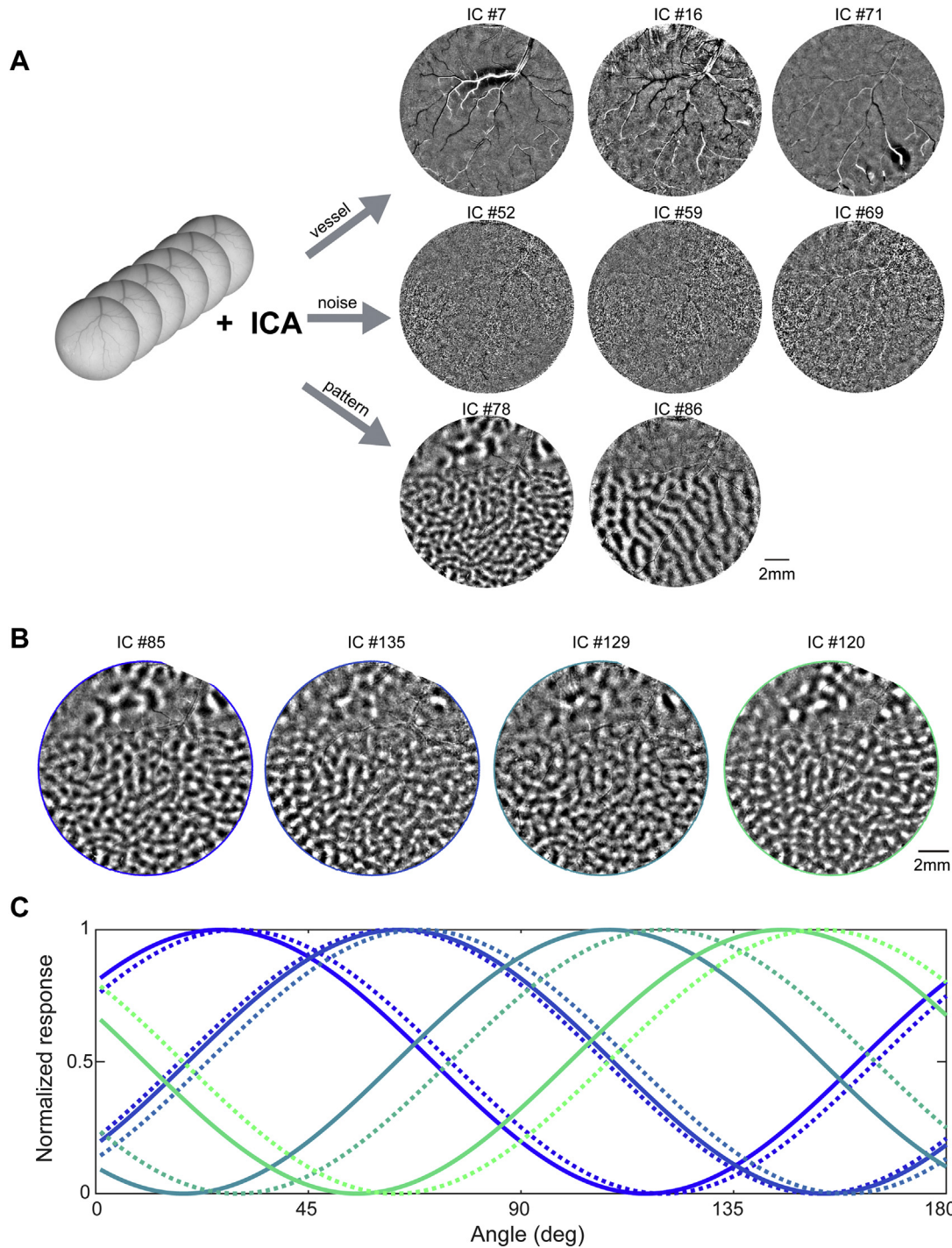


Fig. 5. ICA analysis results. A. An example case analyzed with ICA. Three types of IC examples are selected from a total of 90 ICs, and they are shown for blood vessel signals (top), high-frequency noise (middle row) and IC functional maps (bottom row). B. More examples of orientation-map-like ICs from the same case. C. Response profiles of 9 orientation-map-like ICs obtained from this case. The response profiles of the 4 example ICs in B were shown here in the same color (solid curves).

two phenomena and variation among individuals may provide a clue for this hypothesis.

The present study used anesthetized animals as a model. Many studies have shown that the observed rsFC depends on the level of anesthetics. Most studies found stronger rsFC under light anesthesia than under deep anesthesia (Hutchison et al., 2014; Li et al., 2014; Lv et al., 2016; Hori et al., 2020; Areshenkov et al., 2021; Card et al., 2022). In a VSD study, spontaneous OD and orientation patterns were weaker in awake conditions than in anesthetized conditions (Omer et al., 2019). How-

ever, using anesthetized animals also has some advantages. For example, they are more stable and suitable for extended examination. They also have minimum motion noises. The hemodynamic FC signals we observed were generally weak. In V1, the dR/R value of averaged peaks was around 0.6×10^{-4} (Fig. S2B), roughly 1/3~1/4 of the stimulus-driven ones ($\sim 2 \times 10^{-4}$). Signal sizes also varied greatly among cases, and formed a wide but continuous distribution in the scatter plot in Fig. 2E (also see Fig. S3C). The values of the lower-end cases were actually indistinguishable from shuffled controls (non-significant cases in

Fig. S3A). Weak cases often did not have meaningful patterns in their recovered maps (Fig. 2E). It is not so obvious what caused the large case variation we observed. It could reflect true individual differences in FC strengths. It could also be due to differences in anesthesia depth. Although efforts were made to maintain similar heart rates and CO₂ levels among cases, these indices were not as accurate as EEG in assessing anesthesia depth. Case variation could also be due to the indirect signals we recorded, i.e. individual differences in neuro-hemodynamic coupling.

In this study, the main analysis was performed on differential signals between paired time courses, which only contained network-specific signals. This might contribute to the observation that different types of networks were largely independent (Fig. 2D). Global signals that were removed in the subtraction procedure could be viewed as network-common activity. It usually had a large amplitude and probably contributes to the BOLD signal detected in resting-state fMRI. In our analysis methods, independent fluctuations among different networks required that these networks are spatially independent. The fact that we did not observe cross-network temporal correlations (Fig. 2D) indicates that there was no biased spatial interaction among these networks. This is consistent with previous observations that multiple feature maps remain largely independent when they co-exist in one area (Bartfeld and Grinvald, 1992; Obermayer and Blasdel, 1993; Yu et al., 2005).

Compared with OD and orientation maps, recovered color maps were generally weaker and had lower correlations with stimulus-driven color maps (Figs. S2C, S3C and S6). This might be due to small domain sizes and asymmetrical color vs. non-color domains in color templates (see Methods). Both factors lead to weaker signal and more noise. Probably also due to the weak signal-noise ratio, spontaneous activity in color domains did not show significant correlation between different areas at the population level. Nevertheless, several cases with relatively stronger recovered color maps (e.g., Fig. S6A, B, E) show weak color patterns in non-seed areas, which suggest that color networks in different areas might fluctuate coherently as well. Indeed, anatomically, projections between color domains in different areas have been demonstrated (Sincich and Horton, 2002; Fang et al., 2022).

In conclusion, we found that submillimeter-resolution FC networks can be revealed by hemodynamic signals. Different types of FC networks coexist in each area and fluctuate independently. However, orientation FC networks activate coherently in different areas and even across two hemispheres. Together, these results demonstrate that resting-state hemodynamic signals contain dynamic FC information at mesoscale.

Ethics approval

All procedures were performed in accordance with the National Institutes of Health Guidelines and were approved by the Institutional Animal Care and Use Committee of Beijing Normal University.

Data availability

An example spontaneous dataset and all preprocessed differential signal time course data and codes are available at the Mendeley dataset. <https://data.mendeley.com/datasets/9wym3sz78m/1>.

Declaration of Competing Interest

The authors declare no conflicts of interest.

Credit authorship contribution statement

Xingya Cai: Conceptualization, Methodology, Investigation, Writing – original draft, Writing – review & editing. **Haoran Xu:** Conceptualization, Methodology, Investigation, Writing – review & editing. **Chao Han:** Investigation. **Peichao Li:** Investigation. **Jiayu Wang:** Investigation. **Rui Zhang:** Investigation. **Rendong Tang:** Investigation. **Chen**

Fang: Investigation. **Kun Yan:** Investigation. **Qianling Song:** Investigation. **Chen Liang:** Investigation. **Haidong D. Lu:** Conceptualization, Methodology, Writing – original draft, Writing – review & editing, Funding acquisition, Resources, Supervision.

Acknowledgments

We thank lab members (J. Lu, Y. Xiao, Z. Yu, H. Ma, Y. Li, P. Li, M. Chen, Y. Fang, J. Hu, S. Zhu) for providing technical assistance. This work was supported by the **National Natural Science Foundation of China** [grant numbers 32271079, 31625012, 31530029, and 31371111].

Supplementary materials

Supplementary material associated with this article can be found, in the online version, at doi:[10.1016/j.neuroimage.2023.120019](https://doi.org/10.1016/j.neuroimage.2023.120019).

References

- Amir, Y., Harel, M., Malach, R., 1993. Cortical hierarchy reflected in the organization of intrinsic connections in macaque monkey visual cortex. *J. Comp. Neurol.* 334, 19–46. doi:[10.1002/cne.903340103](https://doi.org/10.1002/cne.903340103).
- Areshenkoff, C.N., Nashed, J.Y., Hutchison, R.M., Hutchison, M., Levy, R., Cook, D.J., Menon, R.S., Everling, S., Gallivan, J.P., 2021. Muting, not fragmentation, of functional brain networks under general anaesthesia. *NeuroImage* 231, 117830. doi:[10.1016/j.neuroimage.2021.117830](https://doi.org/10.1016/j.neuroimage.2021.117830).
- Arieli, A., Sterkin, A., Grinvald, A., Aertsen, A., 1996. Dynamics of ongoing activity: explanation of the large variability in evoked cortical responses. *Science* 273, 1868–1871. doi:[10.1126/science.273.5283.1868](https://doi.org/10.1126/science.273.5283.1868).
- Basole, A., White, L.E., Fitzpatrick, D., 2003. Mapping multiple features in the population response of visual cortex. *Nature* 423, 986–990. doi:[10.1038/nature01721](https://doi.org/10.1038/nature01721).
- Bartfeld, E., Grinvald, A., 1992. Relationships between orientation-preference pinwheels, cytochrome oxidase blobs, and ocular-dominance columns in primate striate cortex. *Proc. Natl. Acad. Sci.* 89, 11905–11909. doi:[10.1073/pnas.89.24.11905](https://doi.org/10.1073/pnas.89.24.11905).
- Bosking, W.H., Zhang, Y., Schofield, B., Fitzpatrick, D., 1997. Orientation selectivity and the arrangement of horizontal connections in tree shrew striate cortex. *J. Neurosci.* 17, 2112–2127. doi:[10.1523/JNEUROSCI.17-06-02112.1997](https://doi.org/10.1523/JNEUROSCI.17-06-02112.1997).
- Card, N.S., Gharabawie, O.A., 2022. Cortical connectivity is embedded in resting state at columnar resolution. *Prog. Neurobiol.* 213, 102263. doi:[10.1016/j.progress.2022.102263](https://doi.org/10.1016/j.progress.2022.102263).
- Chen, M., Li, P., Zhu, S., Han, C., Xu, H., Fang, Y., Hu, J., Roe, A.W., Lu, H.D., 2016. An orientation map for motion boundaries in macaque V2. *Cereb. Cortex* 26, 279–287. doi:[10.1093/cercor/bhu235](https://doi.org/10.1093/cercor/bhu235).
- Fang, C., Yan, K., Liang, C., Wang, J., Cai, X., Zhang, R., Lu, H.D., 2022. Function-specific projections from V2 to V4 in macaques. *Brain Struct. Funct.* 227, 1317–1330. doi:[10.1007/s00429-021-02440-3](https://doi.org/10.1007/s00429-021-02440-3).
- Cusick, C.G., Kaas, J.H., Lepore, F., Ptito, M., Jasper, H.H., 1986. Interhemispheric connections of cortical sensory and motor representations in primates. In: *Two Hemispheres-One Brain: Functions of the Corpus Callosum*. Alan R. Liss, New York, pp. 83–102.
- Fox, M.D., Raichle, M.E., 2007. Spontaneous fluctuations in brain activity observed with functional magnetic resonance imaging. *Nat. Rev. Neurosci.* 8, 700–711. doi:[10.1038/nrn2201](https://doi.org/10.1038/nrn2201).
- Grinvald, A., Shoham, D., Shmuel, A., Glaser, D., Vanzetta, I., Shtoyerman, E., Slovin, H., Wijnenberg, C., Hildesheim, R., Arieli, A., Windhorst, U., Johansson, H., 1999. *In-vivo* optical imaging of cortical architecture and dynamics. In: *Modern Techniques in Neuroscience Research*. Springer Berlin Heidelberg, Berlin, Heidelberg, pp. 893–969. doi:[10.1007/978-3-642-58552-4_34](https://doi.org/10.1007/978-3-642-58552-4_34).
- Hori, Y., Schaeffer, D.J., Gilbert, K.M., Hayrynen, L.K., Cléry, J.C., Gati, J.S., Menon, R.S., Everling, S., 2020. Altered resting-state functional connectivity between awake and isoflurane anesthetized marmosets. *Cereb. Cortex* 30, 5943–5959. doi:[10.1093/cercor/bcaa168](https://doi.org/10.1093/cercor/bcaa168).
- Houzel, J.C., Carvalho, M.L., Lent, R., 2002. Interhemispheric connections between primary visual areas: beyond the midline rule. *Braz. J. Med. Biol. Res.* 35, 1441–1453. doi:[10.1590/s0100-879x2002001200005](https://doi.org/10.1590/s0100-879x2002001200005).
- Hu, J.M., Roe, A.W., 2022. Functionally specific and sparse domain-based micro-networks in monkey V1 and V2. *Curr. Biol.* 32, 2797–2809. doi:[10.1016/j.cub.2022.04.095](https://doi.org/10.1016/j.cub.2022.04.095), e3.
- Hutchison, R.M., Culham, J.C., Flanagan, J.R., Everling, S., Gallivan, J.P., 2015. Functional subdivisions of medial parieto-occipital cortex in humans and nonhuman primates using resting-state fMRI. *NeuroImage* 116, 10–29. doi:[10.1016/j.neuroimage.2015.04.068](https://doi.org/10.1016/j.neuroimage.2015.04.068).
- Hutchison, R.M., Everling, S., 2012. Monkey in the middle: why non-human primates are needed to bridge the gap in resting-state investigations. *Front. Neuroanat.* 6.
- Hutchison, R.M., Hutchison, M., Manning, K.Y., Menon, R.S., Everling, S., 2014. Isoflurane induces dose-dependent alterations in the cortical connectivity profiles and dynamic properties of the brain's functional architecture. *Hum. Brain Mapp.* 35, 5754–5775. doi:[10.1002/hbm.22583](https://doi.org/10.1002/hbm.22583).
- Hyvärinen, A., Oja, E., 2000. Independent component analysis: algorithms and applications. *Neural Netw.* 13, 411–430. doi:[10.1016/S0893-6080\(00\)00026-5](https://doi.org/10.1016/S0893-6080(00)00026-5).

- Innocenti, G.M., Schmidt, K., Milleret, C., Fabri, M., Knyazeva, M.G., Battaglia-Mayer, A., Aboitiz, F., Ptito, M., Caleo, M., Marzi, C.A., Barakovic, M., Lepore, F., Caminiti, R., 2022. The functional characterization of callosal connections. *Prog. Neurobiol.* 208, 102186. doi:[10.1016/j.pneurobio.2021.102186](https://doi.org/10.1016/j.pneurobio.2021.102186).
- Jbabdi, S., Sotiroopoulos, S.N., Behrens, T.E., 2013. The topographic connectome. *Curr. Opin. Neurobiol.* 23, 207–215. doi:[10.1016/j.conb.2012.12.004](https://doi.org/10.1016/j.conb.2012.12.004).
- Li, B., Liu, R., Huang, Q., Lu, J., Luo, Q., Li, P., 2014. Coherent slow cortical potentials reveal a superior localization of resting-state functional connectivity using voltage-sensitive dye imaging. *NeuroImage* 91, 162–168. doi:[10.1016/j.neuroimage.2014.01.004](https://doi.org/10.1016/j.neuroimage.2014.01.004).
- Li, P., Zhu, S., Chen, M., Han, C., Xu, H., Hu, J., Fang, Y., Lu, H.D., 2013. A motion direction preference map in monkey V4. *Neuron* 78, 376–388. doi:[10.1016/j.neuron.2013.02.024](https://doi.org/10.1016/j.neuron.2013.02.024).
- Li, X., Zhu, Q., Vanduffel, W., 2022. Submillimeter fMRI reveals an extensive, fine-grained and functionally-relevant scene-processing network in monkeys. *Prog. Neurobiol.* 211, 102230. doi:[10.1016/j.pneurobio.2022.102230](https://doi.org/10.1016/j.pneurobio.2022.102230).
- Livingstone, M., Hubel, D., 1984. Specificity of intrinsic connections in primate primary visual cortex. *J. Neurosci.* 4, 2830. doi:[10.1523/JNEUROSCI.04-11-02830.1984](https://doi.org/10.1523/JNEUROSCI.04-11-02830.1984).
- Lu, H.D., Chen, G., Cai, J., Roe, A.W., 2017. Intrinsic signal optical imaging of visual brain activity: tracking of fast cortical dynamics. *NeuroImage* 148, 160–168. doi:[10.1016/j.neuroimage.2017.01.006](https://doi.org/10.1016/j.neuroimage.2017.01.006).
- Lu, H.D., Chen, G., Tanigawa, H., Roe, A.W., 2010. A motion direction map in macaque V2. *Neuron* 68, 1002–1013. doi:[10.1016/j.neuron.2010.11.020](https://doi.org/10.1016/j.neuron.2010.11.020).
- Lv, P., Xiao, Y., Liu, B., Wang, Y., Zhang, X., Sun, H., Li, F., Yao, L., Zhang, W., Liu, L., Gao, X., Wu, M., Tang, Y., Chen, Q., Gong, Q., Lui, S., 2016. Dose-dependent effects of isoflurane on regional activity and neural network function: a resting-state fMRI study of 14 rhesus monkeys: an observational study. *Neurosci. Lett.* 611, 116–122. doi:[10.1016/j.neulet.2015.11.037](https://doi.org/10.1016/j.neulet.2015.11.037).
- Malach, R., Amir, Y., Harel, M., Grinvald, A., 1993. Relationship between intrinsic connections and functional architecture revealed by optical imaging and *in vivo* targeted biocytin injections in primate striate cortex. *Proc. Natl. Acad. Sci.* 90, 10469–10473. doi:[10.1073/pnas.90.22.10469](https://doi.org/10.1073/pnas.90.22.10469).
- Malach, R., Tootell, R.B.H., Malonek, D., 1994. Relationship between orientation domains, cytochrome oxidase stripes, and intrinsic horizontal connections in squirrel monkey area V2. *Cereb. Cortex* 4, 151–165. doi:[10.1093/cercor/4.2.151](https://doi.org/10.1093/cercor/4.2.151).
- Mars, R.B., Sallet, J., Neubert, F.-X., Rushworth, M.F.S., 2013. Connectivity profiles reveal the relationship between brain areas for social cognition in human and monkey temporoparietal cortex. *Proc. Natl. Acad. Sci.* 110, 10806–10811. doi:[10.1073/pnas.1302956110](https://doi.org/10.1073/pnas.1302956110).
- Matsui, T., Tamura, K., Koyano, K.W., Takeuchi, D., Adachi, Y., Osada, T., Miyashita, Y., 2011. Direct comparison of spontaneous functional connectivity and effective connectivity measured by intracortical microstimulation: an fMRI study in macaque monkeys. *Cereb. Cortex* 21, 2348–2356. doi:[10.1093/cercor/bhr019](https://doi.org/10.1093/cercor/bhr019).
- Obermayer, K., Blasdel, G., 1993. Geometry of orientation and ocular dominance columns in monkey striate cortex. *J. Neurosci.* 13, 4114. doi:[10.1523/JNEUROSCI.13-10-04114.1993](https://doi.org/10.1523/JNEUROSCI.13-10-04114.1993).
- Omer, D.B., Fekete, T., Ulchin, Y., Hildesheim, R., Grinvald, A., 2019. Dynamic patterns of spontaneous ongoing activity in the visual cortex of anesthetized and awake monkeys are different. *Cereb. Cortex* 29, 1291–1304. doi:[10.1093/cercor/bhy099](https://doi.org/10.1093/cercor/bhy099).
- Rochefort, N.L., Buzás, P., Kisvárday, Z.F., Eysel, U.T., Milleret, C., 2007. Layout of transcallosal activity in cat visual cortex revealed by optical imaging. *NeuroImage* 36, 804–821. doi:[10.1016/j.neuroimage.2007.03.006](https://doi.org/10.1016/j.neuroimage.2007.03.006).
- Schölvinck, M.L., Friston, K.J., Rees, G., 2012. The influence of spontaneous activity on stimulus processing in primary visual cortex. *NeuroImage* 59, 2700–2708. doi:[10.1016/j.neuroimage.2011.10.066](https://doi.org/10.1016/j.neuroimage.2011.10.066).
- Schwiedrzik, C.M., Zarco, W., Everling, S., Freiwald, W.A., 2015. Face patch resting state networks link face processing to social cognition. *PLoS Biol.* 13, e1002245. doi:[10.1371/journal.pbio.1002245](https://doi.org/10.1371/journal.pbio.1002245).
- Sincich, L.C., Horton, J.C., 2002. Divided by cytochrome oxidase: a map of the projections from V1 to V2 in macaques. *Science* 295, 1734–1737. doi:[10.1126/science.1067902](https://doi.org/10.1126/science.1067902).
- Smith, G.B., Hein, B., Whitney, D.E., Fitzpatrick, D., Kaschube, M., 2018. Distributed network interactions and their emergence in developing neocortex. *Nat. Neurosci.* 21, 1600–1608. doi:[10.1038/s41593-018-0247-5](https://doi.org/10.1038/s41593-018-0247-5).
- Stettler, D.D., Das, A., Bennett, J., Gilbert, C.D., 2002. Lateral connectivity and contextual interactions in macaque primary visual cortex. *Neuron* 36, 739–750. doi:[10.1016/S0896-6273\(02\)01029-2](https://doi.org/10.1016/S0896-6273(02)01029-2).
- Tang, R., Song, Q., Li, Y., Zhang, R., Cai, X., Lu, H., 2020. Curvature-processing domains in primate V4. *eLife* 9, doi:[10.7554/eLife.57502](https://doi.org/10.7554/eLife.57502).
- Tsodyks, M., Kenet, T., Grinvald, A., Arieli, A., 1999. Linking spontaneous activity of single cortical neurons and the underlying functional architecture. *Science* 286, 1943–1946. doi:[10.1126/science.286.5446.1943](https://doi.org/10.1126/science.286.5446.1943).
- Vasireddi, A.K., Vazquez, A.L., Whitney, D.E., Fukuda, M., Kim, S.G., 2016. Functional connectivity of resting hemodynamic signals in submillimeter orientation columns of the visual cortex. *Brain Connect* 6, 596–606. doi:[10.1089/brain.2015.0414](https://doi.org/10.1089/brain.2015.0414).
- Vincent, J.L., Patel, G.H., Fox, M.D., Snyder, A.Z., Baker, J.T., Van Essen, D.C., Zempel, J.M., Snyder, L.H., Corbetta, M., Raichle, M.E., 2007. Intrinsic functional architecture in the anaesthetized monkey brain. *Nature* 447, 83–86. doi:[10.1038/nature05758](https://doi.org/10.1038/nature05758).
- Wang, Z., Chen, L.M., Négyessy, L., Friedman, R.M., Mishra, A., Gore, J.C., Roe, A.W., 2013. The relationship of anatomical and functional connectivity to resting-state connectivity in primate somatosensory cortex. *Neuron* 78, 1116–1126.
- White, B.R., Bauer, A.Q., Snyder, A.Z., Schlaggar, B.L., Lee, J.-M., Culver, J.P., 2011. Imaging of functional connectivity in the mouse brain. *PLoS One* 6, e16322. doi:[10.1371/journal.pone.0016322](https://doi.org/10.1371/journal.pone.0016322).
- Wig, G.S., Laumann, T.O., Petersen, S.E., 2014. An approach for parcellating human cortical areas using resting-state correlations. *NeuroImage* 93, 276–291. doi:[10.1016/j.neuroimage.2013.07.035](https://doi.org/10.1016/j.neuroimage.2013.07.035).
- Xiao, Y., Rao, R., Cecchi, G., Kaplan, E., 2008. Improved mapping of information distribution across the cortical surface with the support vector machine. *Neural Netw.* 21, 341–348. doi:[10.1016/j.neunet.2007.12.022](https://doi.org/10.1016/j.neunet.2007.12.022).
- Xu, H., Han, C., Chen, M., Li, P., Zhu, S., Fang, Y., Hu, J., Ma, H., Lu, H.D., 2016. Rivalry-like neural activity in primary visual cortex in anesthetized monkeys. *J. Neurosci.* 36, 3231. doi:[10.1523/JNEUROSCI.3660-15.2016](https://doi.org/10.1523/JNEUROSCI.3660-15.2016).
- Yabuta, N.H., Callaway, E.M., 1998. Cytochrome-oxidase blobs and intrinsic horizontal connections of layer 2/3 pyramidal neurons in primate V1. *Vis. Neurosci.* 15, 1007–1027. doi:[10.1017/S0952523898156018](https://doi.org/10.1017/S0952523898156018).
- Yoshioka, T., Blasdel, G.G., Levitt, J.B., Lund, J.S., 1996. Relation between patterns of intrinsic lateral connectivity, ocular dominance, and cytochrome oxidase-reactive regions in macaque monkey striate cortex. *Cereb. Cortex* 6, 297–310. doi:[10.1093/cercor/6.2.297](https://doi.org/10.1093/cercor/6.2.297).
- Yu, H., Farley, B.J., Jin, D.Z., Sur, M., 2005. The coordinated mapping of visual space and response features in visual cortex. *Neuron* 47, 267–280. doi:[10.1016/j.neuron.2005.06.011](https://doi.org/10.1016/j.neuron.2005.06.011).